Title

GluN3A subunit tunes NMDA receptor synaptic trafficking and content during postnatal brain development.

Journal

Cell Reports, 42(5)

Authors

González-González, Inmaculada

Gray, John

Ferreira, Joana

et al.

Publication Date

2023-05-30

DOI

10.1016/j.celrep.2023.112477

Peer reviewed

HHS Public Access

Author manuscript

Cell Rep. Author manuscript; available in PMC 2024 June 20.

Published in final edited form as:

Cell Rep. 2023 May 30; 42(5): 112477. doi:10.1016/j.celrep.2023.112477.

GluN3A subunit tunes NMDA receptor synaptic trafficking and content during postnatal brain development

Inmaculada M. González-González[1,2], **John A. Gray**[3], **Joana Ferreira**[2], **María Jose Conde-Dusman**[1,4], **Delphine Bouchet**[2], **Isabel Perez-Otaño**[1,4,5,*], **Laurent Groc**[2,*]

[1]Cellular Neurobiology Laboratory, Centro de Investigación Médica Aplicada (CIMA) and Universidad de Navarra, Pamplona, Spain

[2]Université de Bordeaux, CNRS, Interdisciplinary Institute for Neuroscience (IINS), UMR 5297, 33000 Bordeaux, France

[3]Department of Neurology, Center for Neuroscience, University of California, Davis, Davis, CA 95618, USA

[4]Cellular and Systems Biology, Instituto de Neurociencias, CSIC-UMH, 03550 San Juan de Alicante, Spain

[5]Lead contact

Abstract

Signaling via *N*-methyl-D-aspartate receptors (NMDARs) is critical for the maturation of glutamatergic synapses, partly through a developmental switch from immature synapses expressing primarily GluN2B- and GluN3A-containing subtypes to GluN2A-rich mature ones. This subunit switch is thought to underlie the synaptic stabilization of NMDARs necessary for neural network consolidation. However, the cellular mechanisms controlling the NMDAR exchange remain unclear. Using a combination of single-molecule and confocal imaging and biochemical and electrophysiological approaches, we show that surface GluN3-NMDARs form a highly diffusive receptor pool that is loosely anchored to synapses. Remarkably, changes in GluN3A subunit expression selectively alter the surface diffusion and synaptic anchoring of GluN2A-but not GluN2B-NMDARs, possibly through altered interactions with cell surface receptors. The effects of GluN3A on NMDAR surface diffusion are restricted to an early time window of postnatal development in rodents, allowing GluN3A subunits to control the timing of NMDAR signaling maturation and neuronal network refinements.

INTRODUCTION

Early in development, the brain is characterized by an enormous turnover of synapses, with continuous formation and elimination of connections. Sensory inputs and neuronal activity later refine this labile circuitry by stabilizing and strengthening specific subsets of

*Correspondence: otano@umh.es (I.P.-O.), laurent.groc@u-bordeaux.fr (L.G.).

AUTHOR CONTRIBUTIONS

I.M.G.-G., J.A.G., J.F., I.P.-O., M.J.C.-D., and D.B. generated resources and performed and analyzed experiments. I.M.G.-G., I.P.-O., and L.G. conceived and supervised the project and designed the experiments. I.M.G.-G., I.P.-O., and L.G. wrote the manuscript.

synapses.[1] This is a fundamental process because it defines precise neuronal circuits from initially redundant connections, which is critical for fine-tuning behavioral and cognitive repertoires. A key event that determines whether individual glutamate synapses mature is the exchange in *N*-methyl-D-aspartate (NMDA) receptor (NMDAR) subtypes and their signaling, but the pathways underpinning this process remain poorly understood. NMDARs are tetraheteromeric combinations of an obligatory GluN1 subunit and various GluN2 (A–D) and GluN3 (A and B) subunits. GluN2 and GluN3 subunits confer distinct biophysical and pharmacological properties to NMDARs and influence their signaling and subcellular distribution.[2,3] In the adult brain, GluN2A-containing NMDARs (GluN2A-NMDARs) are more concentrated in postsynaptic densities (PSDs) relative to GluN2B-NMDARs, which are found at both synaptic and extrasynaptic locations.[2,4] The expression levels of GluN2A subunits increase over postnatal development, promoting the substitution of GluN2B-NMDARs, which are highly expressed from birth, with GluN2A-NMDARs, which become expressed in virtually every CNS region by adulthood.[5–8] The incorporation of GluN2A-NMDARs into maturing synapses shortens the duration of NMDAR-mediated currents, changing the temporal integration of synaptic inputs, and ultimately affects how synapses are modified by experience.[5,9–11]

Most studies have focused on the roles of the developmental GluN2B-to-GluN2A subunit switch on the maturation of excitatory synapses and neural circuits. However, GluN3A subunits exhibit a distinctive profile of expression, which peaks during postnatal periods when massive synapse stabilization and elimination are taking place and is largely downregulated afterward.[3,12,13] The time course of GluN3A subunit expression and downregulation varies across brain regions, cortical layers, and sensory modalities, matching the timing of synapse and circuit maturation, and is influenced by sensory experience.[14,15] Artificially prolonging GluN3A expression beyond the physiological time window inhibits synapse maturation, promotes pruning, and interferes with the consolidation of memories.[16–18] Conversely, GluN3A subunit deletion is associated with accelerated maturation and enhanced learning.[16–19] Thus, GluN3A-NMDARs are likely key molecular switches for experience-dependent synapse maturation in the juvenile brain. While the mechanisms involved remain unclear, a distinguishing feature of GluN3A-NMDARs is their lesser concentration at PSDs relative to GluN2A- or GluN2B-NMDARs when assessed by electron microscopy or biochemical fractionation, likely related to the lack of classical PDZ-binding motifs.[20,21]

Once in the plasma membrane, NMDARs exchange by lateral diffusion between the extrasynaptic compartment and synapses, where they can be stably or transiently trapped.[22] The rate of receptor diffusion and the receptor affinity for transmembrane and intracellular scaffolds determine their distribution in synaptic and extrasynaptic sites.[23–27] For instance, GluN2A-NMDARs are less mobile and more retained within synapses than GluN2B-NMDARs.[27] Overexpression of GluN2A subunits in cultured neurons decreases the surface diffusion of GluN2B-NMDARs, suggesting a dominant role for GluN2A in the surface dynamics of putative triheteromeric NMDARs.[27] Whether GluN3A subunits influence these parameters to favor an immature NMDAR phenotype at synapses has, however, not been explored. To address this question, we tracked surface GluN3A-NMDARs in live hippocampal neurons and evaluated the impact of GluN3A subunit levels on synaptic

NMDAR surface dynamics. Applying a combination of single nanoparticle imaging, immunohistochemical, electrophysiological, and biochemical approaches, we unveil the dynamics of GluN3A-NMDARs and their impact on the synaptic content of NMDARs in developing neurons.

RESULTS

GluN3A-NMDAR surface dynamics and its regulation by neuronal activity

We first investigated the behavior of GluN3A-NMDARs in cultured hippocampal neurons. A single-nanoparticle (quantum dot [QD]) tracking approach was used to follow individual GFP-tagged GluN3A-NMDARs at the surface of live neurons (Figure 1A). Single QD-GluN3A-NMDARs were homogeneously observed at the dendritic surface of neurons (Figure 1A). To further investigate the diffusion properties of the receptor, we measured the area explored over time by calculating the mean square displacement (MSD) vs. time lag (Figure 1B). The MSD curve of GluN3A-NMDARs indicates that the receptors diffuse in a confined manner at the surface of neurons (Figure 1B). We next monitored the dynamics of GluN3A-NMDARs within glutamatergic synapses identified by the expression of the postsynaptic protein Homer 1-DsRed. As exemplified in Figure 1C, single GluN3A-NMDARs briefly explore the postsynaptic membrane (Homer 1 clusters, in blue) and are mostly observed in extrasynaptic compartments, in agreement with previous observations.[20] We analyzed the trajectories of single synaptic GluN3A-NMDARs (located within and in the 300-nm annulus surrounding Homer 1-DsRed areas) from image frames acquired at 20 Hz and calculated their instantaneous diffusion coefficient and the fraction of immobile receptors (diffusion coefficient <0.005 $\mu m^2/s$). The instantaneous diffusion coefficient is calculated from the first points of the MSD curve (Figure 1B), as classically performed (see STAR Methods). Strikingly, the diffusion of synaptic GluN3A-NMDARs did not differ from their extrasynaptic counterparts, with similar fractions of immobile and comparable diffusion coefficient of mobile GluN3A-NMDAR in synaptic (16% of immobile receptors) and extrasynaptic (15% of immobile receptors) compartments (Figure 1D).

The lack of synaptic concentration could result from reduced anchoring of the receptor in the synapse, which is characterized by a high diffusion in this area. To address this, we compared the dynamics of synaptic GluN3A-NMDARs with GluN2A- and GluN2B-NMDARs (Figure 1E). GluN3A-NMDARs displayed high lateral mobility within the synaptic area compared with GluN2A- and GluN2B-NMDARs, and the proportion of immobile receptors was much lower (16%) than for either GluN2A- or GluN2B-NMDARs (64% and 36%, respectively) (Figures 1F and S1A). The diffusion coefficients were significantly different between receptor subtypes, with GluN2A-NMDAR values lower than those of GluN2B-NMDAR and GluN3A-NMDAR (Figure 1G). Note that the diffusion coefficients of mobile receptors were also significantly different (GluN2A = 0.16 ± 0.005 $\mu m^2/s$, n = 360; GluN2B = 0.32 ± 0.011 $\mu m^2/s$, n = 984; GluN3A = 0.10 ± 0.005 $\mu m^2/s$, n = 476, $p < 0.01$; mean ± SEM). These data indicate that GluN3A-NMDARs are less stabilized within the postsynaptic compartment than GluN2A- or GluN2B-NMDARs. Another possibility is that GluN3A-NMDARs do not concentrate in synapses due to restrictions of access to the postsynapse. To test this, we measured the frequency of exchange

of single GluN3A-NMDARs between the extrasynaptic and synaptic compartments and compared this value with GluN2B-NMDARs. Exchange frequencies were higher for GluN3A-NMDARs (Figure S1B), indicating that GluN3A-NMDARs enter the postsynaptic area at least as efficiently as GluN2B-NMDARs. The faster exchange rate supported the notion that GluN3A-NMDARs form part of a mobile receptor pool loosely anchored to synapses, in line with the low enrichment of GluN3A subunits in detergent-insoluble PSD fractions[21] and their preferential extrasynaptic distribution.[20] Taken together, our data show that GluN3A-NMDARs are highly mobile at the neuronal surface and their mobility is poorly constrained within the synaptic compartment, unlike for GluN2-NMDARs.[23] We finally tested whether GluN3A-NMDAR surface dynamics are sensitive to neuronal network activity, as demonstrated for other NMDAR subtypes.[28] For this, neurons were treated with either bicuculline (20 μM) or tetrodotoxin (TTX) (1 μM) to increase or decrease neuronal activity, respectively. GluN3A-NMDAR surface dynamics was significantly altered by these treatments, with overall reduced surface diffusion in both conditions (Figure 1H). The fraction of immobile receptors increased in both pharmacological conditions, and the diffusion coefficient of mobile receptors decreased in presence of TTX (control = 0.084 ± 0.007 $\mu m^2/s$, n = 239; bicuculline = 0.048 ± 0.008 $\mu m^2/s$, n = 42, $p > 0.05$; TTX = 0.037 ± 0.008 $\mu m^2/s$, n = 112, $p < 0.01$; mean ± SEM). Collectively, we show that GluN3A-NMDARs are highly dynamic at the plasma membrane of hippocampal neurons in an activity-dependent manner.

GluN3A subunit expression regulates surface GluN2A-NMDAR dynamics

We next investigated whether GluN3A subunit expression influences the surface dynamics of other synaptic NMDAR subtypes, such as GluN2A- and GluN2B-NMDARs. For this, GluN3A subunit levels were up- or downregulated in immature hippocampal neurons (7–9 days in vitro [DIV]). Consistent with previous reports,[27] the surface diffusion of synaptic GluN2A-NMDARs was lower than that of GluN2B-NMDARs (Figures 2A–2C). Surprisingly, GluN3A subunit overexpression caused a large increase in the diffusion of synaptic GluN2A-NMDARs without affecting GluN2B-NMDARs (Figures 2A and 2B). The effect was due to changes in both the proportion of immobile GluN2A-NMDARs and the diffusion of mobile receptors. GluN3A subunit overexpression decreased the fraction of immobile GluN2A-NMDARs by 2-fold (51% in control vs. 23% in GluN3A subunit-expressing neurons; Figure 2B). Noteworthy, the fraction of immobile synaptic GluN2A-NMDARs became similar to the one of GluN3A-NMDARs (see Figures 1D and 2B). The diffusion coefficient of mobile GluN2A-NMDARs doubled with GluN3A subunit overexpression (control = 0.10 ± 0.016 $\mu m^2/s$, n = 89; GluN3A-transfected = 0.19 ± 0.016 $\mu m^2/s$, n = 119; $p < 0.0001$). In line with this, GluN3A subunit overexpression facilitated the exchange of GluN2A-NMDARs between synaptic and extrasynaptic locations and decreased the time spent by GluN2A-NMDARs in the synaptic compartment (Figures S2A and S2B).

Reducing GluN3A subunit levels using two validated short hairpin RNAs (shRNAs)[17,29] had opposite effects on GluN2A-NMDAR surface dynamics. The diffusion of synaptic GluN2A-NMDARs was decreased in neurons expressing either sh1185 or sh2532 shRNA (Figures 2C and 2D), and their synaptic residency time was significantly increased (Figure S2C). This effect was mostly due to an increased fraction of immobile GluN2A-NMDARs (49%in

control vs. 66% and 70% in sh1185 or sh2532 respectively; Figure 2D) since GluN3A subunit knockdown did not significantly reduce the diffusion of mobile GluN2A-NMDARs (control = 0.12 ± 0.006 $\mu m^2/s$, n = 85; sh1185 = 0.13 ± 0.011 $\mu m^2/s$, n = 209; sh2532 = 0.12 ± 0.008 $\mu m^2/s$, n = 240; $p > 0.05$). The diffusion of GluN2B-NMDARs was not affected by either shRNA (Figures 2D and 2E). Thus, the expression level of GluN3A subunit bidirectionally and selectively regulates the surface dynamics of synaptic GluN2A-NMDARs.

Recent work shows that, despite the major postnatal downregulation, significant GluN3A subunit levels are retained in specific brain regions into adulthood.[13,15,30] Thus we asked whether GluN3A subunit expression similarly affects GluN2A-NMDAR surface dynamics in mature hippocampal neurons (>15–18 DIV), when the expression of GluN2A subunits and scaffolding proteins such as PSD95 has reached adult levels.[31] GluN3A overexpression selectively increased the diffusion of synaptic GluN2A-NMDARs and decreased the fraction of immobile receptors (Figures S3A and S3B), indicating that GluN3A subunits can "destabilize" synaptic GluN2A-NMDARs in mature neurons as efficiently as in immature ones. The synaptic confinement of GluN2A-NMDARs was strongly reduced, as illustrated by changes in the MSD curve in neurons overexpressing GluN3A subunit (Figure S3C). We then measured the impact of GluN3A subunit knockdown. No effects on GluN2A-NMDAR surface dynamics or MSD curves were observed (Figure S4), likely reflecting the natural downregulation of endogenous GluN3A subunits at this stage. Thus, re-expression of GluN3A subunits in mature hippocampal networks is sufficient to modify the diffusion properties of GluN2A-NMDARs and confer enhanced mobility.

The above data demonstrate that GluN3A subunits regulate the surface dynamics of GluN2A-NMDARs. The most parsimonious explanation would be that the GluN3A subunit assembles with a fraction of GluN2A subunits to form GluN1/GluN2A/GluN3A triheteromers with diffusion properties that differ from GluN1/GluN2A NMDARs. Addressing this point is not trivial as it would require the biochemical identification and dynamics properties of such triheteromeric complex in live synapses. To circumvent this difficulty, we first verified that GluN3A subunit associates with GluN2A subunits in young hippocampal neurons using co-immunoprecipitation experiments (Figure 3A). Then, to directly address whether GluN3A and GluN2A subunits form complexes at the neuronal surface, we used a surface crosslinking (x-link) assay.[28,32] This allowed us to assess the rapid impact of GluN3A surface dynamics on other NMDAR subtypes. Neurons expressing GFP-GluN3A were exposed to an antibody against the extracellular GFP tag, followed by specific secondary antibodies to x-link surface GluN3A-NMDARs (Figure 3B). Then, the surface dynamics of GluN2A-NMDARs was imaged with the assumption that, if GluN3A subunit alters surface GluN2A-NMDARs, x-linking will unveil this process. The surface x-link of GluN3A subunit strongly reduced its own diffusion, validating the robustness of the protocol (Figures 3C and S5). In addition, the surface immobilization of GluN3A subunits rapidly reduced the surface diffusion of both synaptic and extrasynaptic GluN2A-NMDARs and prevented the destabilizing effects of GluN3A subunit overexpression on synaptic GluN2A-NMDARs (Figure 3D). In basal conditions, 57% of GluN2A-NMDARs were immobile, whereas this value increased to 87% upon GluN3A x-link (no significant change in mobile receptor diffusion coefficient; Figure 3E). The same GluN3A x-link did

not alter GluN2B-NMDAR surface dynamics (Figure S5B). We then performed the reverse experiment in which GluN2A- or GluN2B-NMDARs were x-linked and GluN3A-NMDAR surface diffusion monitored. GluN2A-NMDAR x-link increased the fraction of immobile GluN3A-NMDAR (no significant change in mobile receptor diffusion coefficient), whereas GluN2B-NMDAR x-linking was without noticeable effect on surface diffusion parameters (Figure 3F). The specificity of the GluN3A x-link effect was further demonstrated by imaging another glutamate receptor (i.e., GluA1-AMPAR). We report no alteration of GluN3A-NMDAR surface diffusion following GluA1-AMPAR surface x-link (Figure 3G). Collectively, these data indicate that GluN3A and GluN2A subunits influence each other at the plasma membrane of immature neurons.

The increase in synaptic GluN2A-NMDAR dynamics triggered by GluN3A subunit expression might be due to weakened interactions with synaptic anchoring partners. Two molecular partners have been associated with the trapping of GluN2A-NMDARs at synapses: the transmembrane EphB2 receptor (EphB2R) and the PDZ scaffold protein PSD95. Both proteins are located at postsynaptic densities and interact directly with NMDARs.[23,24,33,34] To test whether GluN3A subunit modifies these interactions, we performed co-immunoprecipitation experiments and quantified the interaction of GluN2A subunits with either EphB2R or PSD95 in wild-type (WT) and GluN3A-null mouse (*Grin3a*$^{-/-}$) hippocampus. The interaction between GluN2A subunit and EphB2R was significantly enhanced in *Grin3a*$^{-/-}$ mice, whereas GluN2A subunit binding to PSD95 was unaffected (Figures S6A and S6B). There was no change when examining complexes with the GluN2B subunit (Figure S6C). These data indicate that, in the absence of GluN3A subunits, EphB2R acts as a strong anchoring partner for GluN2A-NMDARs, whereas PSD95 interaction does not regulate GluN3A-dependent anchoring of GluN2A-NMDARs. Collectively, these data support a model in which the EphB2R-dependent stabilization of GluN2A-NMDARs at maturing synapses is regulated by GluN3A subunits.

GluN3A subunits developmentally alter synaptic GluN2A-NMDAR content

We finally investigated whether GluN3A subunit expression affects the synaptic content of GluN2A-NMDARs, as could be predicted from the selective effect on surface diffusion. We first analyzed the localization of GluN2A and GluN2B subunits within postsynaptic areas (labeled with Homer 1c) in hippocampal neurons from WT and *Grin3a*$^{-/-}$ mice using quantitative immunofluorescence. The fraction of GluN2A-NMDARs at *Grin3a*$^{-/-}$ synapses was significantly increased compared with WT synapses at times of high endogenous GluN3A expression (9 DIV; Figure 4A). In contrast, no difference in the number of Homer1c clusters containing GluN2B subunits was detected (Figure 4B). In mature neurons (15–18 DIV), GluN2A subunit content did not differ between WT and *Grin3a*$^{-/-}$ synapses, consistent with the low GluN3A expression levels and with the lack of effect of GluN3A silencing on GluN2A or 2B subunit mobility at this stage (Figures 4C and 4D). To directly test whether the GluN3A subunit is sufficient to drive the exchange in synaptic GluN2-NMDARs, we expressed GFP-GluN3A in mature *Grin3a*$^{-/-}$ neurons. Re-expression of GluN3A subunit decreased the synaptic content of GluN2A-NMDARs, which reverted to values similar to those observed in younger cultures (Figure 4C). The effect was GluN2A subunit-specific since synaptic GluN2B-NMDARs remained unchanged (Figure 4D).

These results demonstrate that GluN3A subunit expression selectively controls GluN2A-NMDAR synaptic abundance. Electrophysiological experiments in CA1 pyramidal cells from organotypic hippocampal slices further confirmed that GluN3A subunit overexpression decreases the synaptic incorporation of GluN2A subunits. Evoked NMDAR-EPSCs recorded from GFP-GluN3A transfected neurons displayed significantly slower decay times relative to un-transfected neighbors (Figure 4E). NMDAR-EPSCs were more sensitive to the GluN2B antagonist Ro25–6981 (Figure 4F), suggesting a lower GluN2A/2B ratio. These data indicate that GluN3A subunits limit GluN2A-NMDAR synaptic enrichment while leaving unaltered GluN2B-NMDAR distribution.

To confirm this observation *in vivo*, we recorded NMDAR-EPCSs in CA1 pyramidal neurons from either WT or *Grin3a*$^{-/-}$ mice and used the GluN2B antagonist ifenprodil to estimate the GluN2B-NMDAR synaptic content through the first 5 weeks of postnatal development. For reference, we included the ifenprodil sensitivity data of “pure” synaptic populations of GluN2A and GluN2B (Figure 4G, green dots, from Gray et al.[35]). Until postnatal day (P) 11, the fraction of GluN2B-NMDARs was undistinguishable between WT and *Grin3a*$^{-/-}$ mice. However, over the second and third postnatal weeks, as GluN2A expression progressively increases,[6] the fraction of GluN2B-NMDARs was reduced in *Grin3a*$^{-/-}$ mice. This matched an increased GluN2A/2B ratio detected by immunoblot analysis in P16 *Grin3a*$^{-/-}$ mice relative to WT (Figure 4H), which was in line with previous work.[16] The effect was transient as differences in the GluN2B-NMDAR synaptic fraction between WT or *Grin3a*$^{-/-}$ mice normalized after P21 (Figure 4G). These data support our model that GluN3A subunit expression restrains the synaptic incorporation of GluN2A-NMDARs over a critical window of postnatal development.

DISCUSSION

The synaptic number of synaptic NMDARs is based on a dynamic equilibrium between receptors entering and exiting the postsynaptic area through lateral diffusion and exo/endocytosis. The set point of this equilibrium depends on interactions with intracellular scaffolds, transmembrane proteins, and extracellular factors that are determined by the receptor subunit composition.[23–26,36] The surface diffusion of synaptic GluN2A-NMDARs is, for instance, lower than that of GluN2B-NMDARs,[27] likely due to difference in anchoring mechanism(s) such as different scaffold proteins.[23–26] Here we show that GluN3A subunits keep GluN2A-NMDARs away from synapses by reducing their confinement and dwell times within the postsynaptic compartment and facilitating receptor exchange between synaptic and extrasynaptic sites. Based on the following evidence, (1) the developmental decrease in GluN3A subunit expression coincides with the progressive incorporation of GluN2A-NMDARs to postsynaptic sites; (2) the high surface diffusion of GluN3ANMDARs and predominance at extrasynaptic sites relative to either GluN2A or GluN2B-NMDARs; and (3) the positive and selective regulation by GluN3A subunits of GluN2A-NMDAR surface diffusion, we propose a model in which the presence of GluN3A subunit “destabilizes” GluN2A-NMDARs at maturing synapses, delaying their stabilization.

Our data suggest a role of EphB2R in the maturation of GluN2-NMDAR signaling at glutamate synapses. Knocking out GluN3A subunits did not alter the binding of GluN2A

subunit to PSD95, arguing that the destabilization of GluN2A-NMDARs by GluN3A subunit is independent of interaction with PSD95. However, knocking out the GluN3A subunit altered the interaction between NMDARs and EphB2R. The EphB2R interacts directly, through extracellular domains, with NMDARs,[33,34,37] and preventing this interaction causes the rapid dispersal of GluN2A-NMDARs toward extrasynaptic sites.[24] Consistently, knocking out EphB2R results in a lower synaptic GluN2A subunit content without affecting surface GluN2A subunit levels.[38] We propose that the destabilization of GluN2A-NMDARs by the GluN3A subunit provides a means to restrict the synaptic GluN2B-to-GluN2A switch to later stages of development and allows the predominance of GluN2B-NMDAR signaling during a critical period of synaptic development and refinement.[35,39–41] The data showing that GluN3A-NMDAR surface diffusion is regulated by neuronal activity further suggest a role of the GluN3A subunit in driving synaptic maturation. Since GluN3A-NMDARs are modulated by a variety of lectins,[42] one cannot exclude that the extracellular matrix also contributes to the GluN3A-dependent maturation of NMDAR signaling. In addition, the GluN3A subunit expression regulated the surface diffusion of GluN2A-but not that of GluN2B-NMDARs. This was somehow surprising as GluN3A subunits have been proposed to assemble with both GluN2A and GluN2B subunits.[18] Possibly, GluN3A subunits when assembled with GluN2B subunit do not interfere with interactions involved in synaptic anchoring.

Altogether, our study unveils a mechanism whereby GluN3A subunits prevent the stabilization of GluN2A-NMDARs at maturing synapses, favoring a low GluN2A/2B synaptic ratio. The developmentally restricted expression of GluN3A subunits would serve as a mechanism to slow down the maturation of glutamatergic synapses and control its coupling to experience, an evolutionary process essential for the proper development of mammalian brains that spans weeks to decades in humans. Recent functional and mRNA expression studies reveal that GluN3A continues to be expressed into adulthood in multiple brain regions and cell types that have in common strong plasticity needs or conduct high-order integration of information.[13,15] The altered GluN3A expression in a variety of neurodevelopmental and psychiatric disorders[43] would thus restrict temporal windows for NMDAR plasticity and synaptic maturation, leading to premature and poorly functional neuronal networks.

Limitations of the study

This study unveils in hippocampal neurons the surface diffusion of GluN3A-NMDARs and its developmental interplay with other GluN2A/2B-NMDARs. The mechanism underpinning the impact of GluN3A subunits on the surface diffusion and organization of other NMDAR subtypes remain, however, to be firmly established. For instance, although our data suggest the presence of membrane triheteromeric complexes, containing GluN1/3A/2A-NMDARs, additional investigations are surely required to shed light on their presence, content, and pharmacology. Furthermore, our characterization of GluN3A-NMDAR surface diffusion has been performed in cultured hippocampal neurons, a powerful artificial network that, however, lacks some structural and regulatory elements. Tracking membrane GluN3A-NMDAR in the intact brain tissue and in other brain structures in which GluN3A-NMDARs are also present at adulthood will be of prime interest.

STAR METHODS

RESOURCE AVAILABILITY

Lead contact—Further information and requests for resources and reagents should be directed to and will be fulfilled by the lead contact, Isabel Pérez-Otaño (otano@umh.es).

Materials availability—This study did not generate any unique reagents

Data and code availability—All data reported in this paper will be shared by the lead contact upon request. This paper does not report original code.

EXPERIMENTAL MODEL AND SUBJECT DETAILS

Cultures of primary hippocampal neurons were prepared from embryonic day 19 Sprague–Dawley rat embryos or postnatal (P0–P2) mice from both sexes. Male and female *Grin3a*$^{-/-}$ and wild-type mice in a C57Bl6/J background were used for neuronal culture, biochemical and electrophysiological studies. All experiments were conducted in strict compliance with European Community Council and Spanish Directives for care of laboratory animals and animal experimentation, the University of Bordeaux/CNRS Animal Care and Use Committee, and University of California San Francisco Institutional Animal Care and Use Committee.

METHOD DETAILS

Neuronal culture and transfection—Cultures of primary hippocampal neurons were prepared from embryonic day 19 Sprague–Dawley rat embryos or postnatal (P0–P2) mice.[46] Both males and females were used. Briefly, hippocampi were dissected and dissociated with papain (Worthington Biochemical). Cells were plated at a density of 25,000–40,000 per well onto 15 mm glass coverslips coated with poly-DL-ornithine (Sigma) and laminin (BD Biosciences), and maintained in Neurobasal medium supplemented with B27 (Invitrogen) and 5% fetal bovine serum (HyClone). Neurons were transfected at 3 or 10–12 DIV with cDNAs using the Effectene transfection reagent (Qiagen). Briefly, 2 μg of DNA were mixed with 25 μl of Effectene and 8 μl of Enhancer in 150 μl of reaction buffer, and the mixture was added to cultured neurons which were transferred to fresh serum-free Neurobasal medium 10 min before transfection. After 45 min, the medium was replaced. Experiments were performed at the indicated ages.

Single nanoparticle (QD) tracking and surface diffusion calculation—For GFP-GluN3A QD tracking, transfected neurons were incubated with anti-GFP antibody (A-11120, Molecular Probes) for 10 min. For endogenous GluN2-QD tracking, hippocampal neurons were incubated with antibody against the N-terminal extracellular domain of GluN2A (Alomone Labs, AGC-002; epitope corresponding to residues 41–53 of GluN2A subunit) or GluN2B subunits (Alomone Labs, AGC-003; epitope corresponding to residues 323–337 of GluN2B subunit) for 10 min. Neurons were then washed and incubated for 5 min with QD 655 donkey anti-mouse or rabbit IgG (Q22088 and Q-11421MP, Invitrogen). For cross-linking experiments, neurons were incubated with highly concentrated (1:20) polyclonal antibody against GFP (Anti-GFP antibody ab5450, Abcam), and an unconjugated

secondary anti-goat (ab6697, Abcam). Non-specific binding was blocked by adding casein (Vector Laboratories) to the QD 15 min before use. QDs were detected using a mercury lamp and appropriate excitation/emission filters. Images were acquired with an interval of 50 ms and up to 500 consecutive frames. Signals were detected using a CCD camera (Quantem; Roper Scientific). QDs were followed on randomly selected dendritic regions for up to 20 min. QD recording sessions were processed with the Metamorph software (Universal Imaging Corp). The instantaneous diffusion coefficient (D) was calculated for each trajectory from linear fits of the first four points of the mean square displacement (MSD) versus time function using $MSD(t) = < r2 > (t) = 4Dt$. To determine the distribution of single QD complexes, frame stacks were obtained and after binarization of the synaptic signal the complexes were automatically located into synaptic (Homer-1c positive area including surrounding 2 pixels) and extrasynaptic compartments. The two-dimensional trajectories of single molecules in the plane of focus were constructed by correlation analysis between consecutive images using a Vogel algorithm. QD-based trajectories were considered synaptic if they colocalized with Homer 1-DsRed dendritic clusters for at least five frames.

Immunocytochemistry—Neurons were fixed in 2% paraformaldehyde, 2% sucrose and stained in non-permeabilized conditions with primary antibodies against extracellular GluN2A or GluN2B (ACG-002 and ACG-003, Alomone). Cells were permeabilized with cold methanol and, after 30 min in blocking solution, incubated with Homer1 antibody (sc-8923, Santa Cruz Biotechnology) for 1h. Cells were washed and incubated with Cy3- or Cy5-conjugated secondary antibodies for 30 min at room temperature prior to visualization by confocal fluorescent microscopy. Co-localization analysis was performed as described in.[47]

Preparation of tissue extracts—Forebrains from male and female mice of different ages (P7–9, P16) were dissected on ice and homogenized with a Polytron in 50mM Tris-HCl, pH 7.4, containing a protease inhibitor mixture (Roche). Membranes were sedimented by centrifugation (100,000 3 g, 30 min, 4°C) and solubilized in 1% deoxycholate (DOC), 50mMTris-HCl, and 1mMEDTA, pH 9, for 45 min at 37°C. Insoluble material was removed by centrifugation. Triton X-100 was added to a final concentration of 0.1%, and the supernatant was dialyzed for 16 hr against 50 mM Tris, pH 7.5, containing 0.1% Triton X-100. Insoluble material was removed by centrifugation, and the supernatant was stored at −80°C until immunoprecipitation reactions were performed.

Immunoprecipitation—Brain extracts were precleared with protein A/G agarose beads (ThermoFisher Scientific) for 1 h at 4°C. Precleared lysates (100–200 μg) were incubated overnight at 4°C with the specific antibody (anti-GluN2A, M264, Sigma; anti-GluN2B, AB1557, Sigma) or appropriate control IgG (Pierce), followed by incubation with protein A/G beads for 2 h at 4°C. Beads were collected by centrifugation and washed three times in lysis buffer. Immunoprecipitated proteins were eluted with SDS sample buffer and separated by SDS/PAGE electrophoresis. Proteins were transferred onto PVDF membranes (GE Healthcare). After incubation with primary antibodies (anti-GluN3A, 07–356, Upstate; anti-GluN2A, M264 Sigma; anti-GluN2B, AB1557, Sigma; anti-PSD95: CP35, Calbiochem;

anti-EphB2R AF467 R&D System), membranes were incubated with secondary HRP-conjugated anti-mouse or anti-rabbit (LNA934V and LNA931V GE Healthcare).

Electrophysiology in organotypic slice cultures—Hippocampal organotypic slice cultures were prepared from 7 day old rats (male and female).[48] Cultured slices were biolistically transfected after 4 days in culture with GFP-GluN3A using a Helios Gene Gun (Bio-Rad) with 1 μm DNA–coated gold particles. Slices were maintained at 34°C with media changes every other day. Slices were recorded in a submersion chamber on an upright Olympus microscope, perfused in room temperature in ACSF containing (in mM) NaCl 125, KCl 2.5, NaH_2PO_4 1.25, $NaHCO_3$ 25, glucose 11, $MgSO_4$ 4 and $CaCl_2$ 4, saturated with 95% O2/5% CO2. The intracellular solution contained (in mM) $CsMeSO_4$ 135, HEPES 10, NaCl 8, EGTA 0.3, Mg-ATP 4, Na-GTP 0.3, QX-314 5. Picrotoxin (0.1 mM) and NBQX (10 μM) were added to the ACSF to block GABAA and AMPA receptors respectively. CA1 pyramidal cells were visualized by infrared differential interference contrast microscopy and transfected neurons were identified by epifluorescence. Recordings were made simultaneously from transfected and control neurons on DIV7 and synaptic currents were evoked by Schaffer collateral stimulation. For all paired recordings, the number of experiments (n) reported in the figure legends refer to the number of pairs. NMDAR-EPSCs were recorded at +40 mV.

Electrophysiology in acute hippocampal slices—Transverse 300 mm hippocampal slices from wild-type and *Grin3a*$^{-/-}$ mice (male and female) were cut on a D.S.K. microslicer DTK-1000 vibrating microtome (Ted Pella, CA) in high sucrose low sodium cutting solution, containing (in mM): KCl 2.5, $CaCl_2$ 0.5, $MgCl_2$ 7, NaH_2PO_4 1.25, $NaHCO_3$ 25, glucose 7 and sucrose 210. Freshly cut slices were placed in an incubating chamber containing artificial cerebrospinal fluid (ACSF), containing (in mM) NaCl 119, KCl 2.5, $NaHCO_3$ 26.2, Na_2PO_4 1, glucose 11, $CaCl_2$ 2.5, $MgCl_2$ 1.3, and recovered at 35°C for ~1h. Slices were then maintained in ACSF at room temperature prior to recording for 0.5–1 h. Slices were then transferred to a submersion chamber on an upright Olympus microscope, perfused in room temperature normal ACSF containing picrotoxin (0.1 mM) and saturated with 95% O2/5% CO2. CA1 pyramidal cells were visualized by infrared differential interference contrast microscopy. The intracellular solution contained (in mM): $CsMeSO_4$ 100, BAPTA-tetracesium 10, NaCl 8, HEPES 10, Na-GTP 0.3, Mg-ATP 4, EGTA 0.3, QX-314 5, and spermine 0.1. Cells were recorded with 3- to 5-MΩ borosilicate glass pipettes, following stimulation of Schaffer collaterals with monopolar glass electrodes filled with ACSF placed in stratum radiatum of the CA1 region. NMDAR-EPSCs were measured at +40 mV in the presence of 10 μM NBQX. For ifenprodil experiments, after obtaining a 5–10 min stable baseline of NMDAR-EPSCs, 3 μM ifenprodil was applied until an asymptote was achieved, generally 30–40 min. BAPTA was included in the intracellular solution to prevent Ca^{2+}-mediated effects during these extended recordings.[49] Series resistance was monitored and not compensated, and cells in which series resistance varied by >20% during a recording session were discarded. Synaptic responses were collected with a Multiclamp 700B-amplifier (Axon Instruments, Foster City, CA), filtered at 2 kHz, digitized at 10 Hz.

QUANTIFICATION AND STATISTICAL ANALYSES

Statistical significance for differences between paired combinations of images was calculated using the two-tailed Student's t-test or Mann Whitney test. Statistical analysis of differences between experimental groups was performed using one-way ANOVA Kruskal-Wallis test followed by post-hoc Dunn's or Tukey test calculated using Sigma Stat software. Data are presented as cumulative frequency or mean ± SEM.

Supplementary Material

Refer to Web version on PubMed Central for supplementary material.

ACKNOWLEDGMENTS

We thank Stuart Lipton and Nobuki Nakanishi for providing *Grin3a*$^{-/-}$ mice. This work was supported by an NARSAD Independent Award, Spanish Ministry of Science (SAF2013-48983-R, SAF2016-80895R), and Generalitat Valenciana grants (Prometeo 2019/020) (to I.P.O.); EMBO Short-term fellowship, Marie Curie IEF (to I.M.G.-G.); Centre National de la Recherche Scientifique (to I.M.G.-G. and L.G.); Fondation Mé dicale de la Recherche (to L.G.); Agence Nationale de la Recherche (to L.G.); and NIH grants K08MH100562 and R01MH117130 (to J.A.G).

REFERENCES

1. Katz LC, and Shatz CJ (1996). Synaptic activity and the construction of cortical circuits. Science 274, 1133–1138. [PubMed: 8895456]
2. Paoletti P, Bellone C, and Zhou Q (2013). NMDA receptor subunit diversity: impact on receptor properties, synaptic plasticity and disease. Nat. Rev. Neurosci 14, 383–400. [PubMed: 23686171]
3. Pérez-Otaño I, Larsen RS, and Wesseling JF (2016). Emerging roles of GluN3-containing NMDA receptors in the CNS. Nat. Rev. Neurosci 17, 623–635. [PubMed: 27558536]
4. Lau CG, and Zukin RS (2007). NMDA receptor trafficking in synaptic plasticity and neuropsychiatric disorders. Nat. Rev. Neurosci 8, 413–426. [PubMed: 17514195]
5. Stocca G, and Vicini S (1998). Increased contribution of NR2A subunit to synaptic NMDA receptors in developing rat cortical neurons. J. Physiol 507, 13–24. [PubMed: 9490809]
6. Sheng M, Cummings J, Roldan LA, Jan YN, and Jan LY (1994). Changing subunit composition of heteromeric NMDA receptors during development of rat cortex. Nature 368, 144–147. [PubMed: 8139656]
7. Rodenas-Ruano A, Chávez AE, Cossio MJ, Castillo PE, and Zukin RS (2012). REST-dependent epigenetic remodeling promotes the developmental switch in synaptic NMDA receptors. Nat. Neurosci 15, 1382–1390. [PubMed: 22960932]
8. Monyer H, Burnashev N, Laurie DJ, Sakmann B, and Seeburg PH (1994). Developmental and regional expression in the rat brain and functional properties of four NMDA receptors. Neuron 12, 529–540. [PubMed: 7512349]
9. Tovar KR, and Westbrook GL (1999). The incorporation of NMDA receptors with a distinct subunit composition at nascent hippocampal synapses in vitro. J. Neurosci 19, 4180–4188. [PubMed: 10234045]
10. Crair MC, and Malenka RC (1995). A critical period for long-term potentiation at thalamocortical synapses. Nature 375, 325–328. [PubMed: 7753197]
11. Philpot BD, Sekhar AK, Shouval HZ, and Bear MF (2001). Visual experience and deprivation bidirectionally modify the composition and function of NMDA receptors in visual cortex. Neuron 29, 157–169. [PubMed: 11182088]
12. Grand T, Abi Gerges S, David M, Diana MA, and Paoletti P (2018). Unmasking GluN1/GluN3A excitatory glycine NMDA receptors. Nat. Commun 9, 4769. [PubMed: 30425244]

13. Otsu Y, Darcq E, Pietrajtis K, Mátyás F, Schwartz E, Bessaih T, Abi Gerges S, Rousseau CV, Grand T, Dieudonné S, et al. (2019). Control of aversion by glycine-gated GluN1/GluN3A NMDA receptors in the adult medial habenula. Science 366, 250–254. [PubMed: 31601771]

14. Larsen RS, Smith IT, Miriyala J, Han JE, Corlew RJ, Smith SL, and Philpot BD (2014). Synapse-specific control of experience-dependent plasticity by presynaptic NMDA receptors. Neuron 83, 879–893. [PubMed: 25144876]

15. Murillo A, Navarro AI, Puelles E, Zhang Y, Petros TJ, and Pérez-Otaño I (2021). Temporal dynamics and neuronal specificity of Grin3a expression in the mouse forebrain. Cereb. Cortex 31, 1914–1926. [PubMed: 33290502]

16. Henson MA, Larsen RS, Lawson SN, Pérez-Otaño I, Nakanishi N, Lipton SA, and Philpot BD (2012). Genetic deletion of NR3A accelerates glutamatergic synapse maturation. PLoS One 7, e42327. [PubMed: 22870318]

17. Kehoe LA, Bellone C, De Roo M, Zandueta A, Dey PN, Pérez-Otaño I, and Muller D (2014). GluN3A promotes dendritic spine pruning and destabilization during postnatal development. J. Neurosci 34, 9213–9221. [PubMed: 25009255]

18. Roberts AC, Díez-García J, Rodriguiz RM, López IP, Luján R, Martínez-Turrillas R, Picó E, Henson MA, Bernardo DR, Jarrett TM, et al. (2009). Downregulation of NR3A-containing NMDARs is required for synapse maturation and memory consolidation. Neuron 63, 342–356. [PubMed: 19679074]

19. Conde-Dusman MJ, Dey PN, Elía-Zudaire Ó, Rabaneda LG, García-Lira C, Grand T, Briz V, Velasco ER, Andero R, Niñerola S, et al. (2021). Control of protein synthesis and memory by GluN3A-NMDA receptors through inhibition of GIT1/mTORC1 assembly. Elife 10, e71575. [PubMed: 34787081]

20. Pérez-Otaño I, Luján R, Tavalin SJ, Plomann M, Modregger J, Liu XB, Jones EG, Heinemann SF, Lo DC, and Ehlers MD (2006). Endocytosis and synaptic removal of NR3A-containing NMDA receptors by PACSIN1/syndapin1. Nat. Neurosci 9, 611–621. [PubMed: 16617342]

21. Martínez-Turrillas R, Puerta E, Chowdhury D, Marco S, Watanabe M, Aguirre N, and Pérez-Otaño I (2012). The NMDA receptor subunit GluN3A protects against 3-nitroproprionic-induced striatal lesions via inhibition of calpain activation. Neurobiol. Dis 48, 290–298. [PubMed: 22801082]

22. Bard L, and Groc L (2011). Glutamate receptor dynamics and protein interaction: lessons from the NMDA receptor. Mol. Cell. Neurosci 48, 298–307. [PubMed: 21640188]

23. Bard L, Sainlos M, Bouchet D, Cousins S, Mikasova L, Breillat C, Stephenson FA, Imperiali B, Choquet D, and Groc L (2010). Dynamic and specific interaction between synaptic NR2-NMDA receptor and PDZ proteins. Proc. Natl. Acad. Sci. USA 107, 19561–19566. [PubMed: 20974938]

24. Mikasova L, De Rossi P, Bouchet D, Georges F, Rogemond V, Didelot A, Meissirel C, Honnorat J, and Groc L (2012). Disrupted surface cross-talk between NMDA and Ephrin-B2 receptors in anti-NMDA encephalitis. Brain 135, 1606–1621. [PubMed: 22544902]

25. Ladepeche L, Dupuis JP, Bouchet D, Doudnikoff E, Yang L, Campagne Y, Bézard E, Hosy E, and Groc L (2013). Single-molecule imaging of the functional crosstalk between surface NMDA and dopamine D1 receptors. Proc. Natl. Acad. Sci. USA 110, 18005–18010. [PubMed: 24127604]

26. Ferreira JS, Papouin T, Ladépeche L, Yao A, Langlais VC, Bouchet D, Dulong J, Mothet JP, Sacchi S, Pollegioni L, et al. (2017). Co-agonists differentially tune GluN2B-NMDA receptor trafficking at hippocampal synapses. Elife 6, e25492. [PubMed: 28598327]

27. Groc L, Heine M, Cousins SL, Stephenson FA, Lounis B, Cognet L, and Choquet D (2006). NMDA receptor surface mobility depends on NR2A-2B subunits. Proc. Natl. Acad. Sci. USA 103, 18769–18774. [PubMed: 17124177]

28. Dupuis JP, Ladépeche L, Seth H, Bard L, Varela J, Mikasova L, Bouchet D, Rogemond V, Honnorat J, Hanse E, and Groc L (2014). Surface dynamics of GluN2B-NMDA receptors controls plasticity of maturing glutamate synapses. EMBO J. 33, 842–861. [PubMed: 24591565]

29. Yuan T, Mameli M, O'Connor EC, Dey PN, Verpelli C, Sala C, Perez-Otano I, Leuscher C, and Bellone C (2013). Expression of cocaine-evoked synaptic plasticity by GluN3A-containing NMDA receptors. Neuron 80, 1025–1038. [PubMed: 24183704]

30. Bossi S, Dhanasobhon D, Ellis-Davies GCR, Frontera J, de Brito Van Velze M, Lourenço J, Murillo A, Luján R, Casado M, Pérez-Otaño I et al. (2022). GluN3A excitatory glycine receptors control adult cortical and amygdalar circuits. Neuron 110, 2438–2454.e8. [PubMed: 35700736]
31. Li JH, Wang YH, Wolfe BB, Krueger KE, Corsi L, Stocca G, and Vicini S (1998). Developmental changes in localization of NMDA receptor subunits in primary cultures of cortical neurons. Eur. J. Neurosci 10, 1704–1715. [PubMed: 9751142]
32. Heine M, Groc L, Frischknecht R, Béïque JC, Lounis B, Rumbaugh G, Huganir RL, Cognet L, and Choquet D (2008). Surface mobility of postsynaptic AMPARs tunes synaptic transmission. Science 320, 201–205. [PubMed: 18403705]
33. Washburn HR, Xia NL, Zhou W, Mao YT, and Dalva MB (2020). Positive surface charge of GluN1 N-terminus mediates the direct interaction with EphB2 and NMDAR mobility. Nat. Commun 11, 570. [PubMed: 31996679]
34. Dalva MB, Takasu MA, Lin MZ, Shamah SM, Hu L, Gale NW, and Greenberg ME (2000). EphB receptors interact with NMDA receptors and regulate excitatory synapse formation. Cell 103, 945–956. [PubMed: 11136979]
35. Gray JA, Shi Y, Usui H, During MJ, Sakimura K, and Nicoll RA (2011). Distinct modes of AMPA receptor suppression at developing synapses by GluN2A and GluN2B: single-cell NMDA receptor subunit deletion in vivo. Neuron 71, 1085–1101. [PubMed: 21943605]
36. Groc L, Choquet D, Stephenson FA, Verrier D, Manzoni OJ, and Chavis P (2007). NMDA receptor surface trafficking and synaptic subunit composition are developmentally regulated by the extracellular matrix protein Reelin. J. Neurosci 27, 10165–10175. [PubMed: 17881522]
37. Henderson JT, Georgiou J, Jia Z, Robertson J, Elowe S, Roder JC, and Pawson T (2001). The receptor tyrosine kinase EphB2 regulates NMDA-dependent synaptic function. Neuron 32, 1041–1056. [PubMed: 11754836]
38. Nolt MJ, Lin Y, Hruska M, Murphy J, Sheffler-Colins SI, Kayser MS, Passer J, Bennett MVL, Zukin RS, and Dalva MB (2011). EphB controls NMDA receptor function and synaptic targeting in a subunit-specific manner. J. Neurosci 31, 5353–5364. [PubMed: 21471370]
39. Wang CC, Held RG, Chang SC, Yang L, Delpire E, Ghosh A, and Hall BJ (2011). A critical role for GluN2B-containing NMDA receptors in cortical development and function. Neuron 72, 789–805. [PubMed: 22153375]
40. Barria A, and Malinow R (2005). NMDA receptor subunit composition controls synaptic plasticity by regulating binding to CaMKII. Neuron 48, 289–301. [PubMed: 16242409]
41. Gambrill AC, and Barria A (2011). NMDA receptor subunit composition controls synaptogenesis and synapse stabilization. Proc. Natl. Acad. Sci. USA 108, 5855–5860. [PubMed: 21427228]
42. Hemelikova K, Kolcheva M, Skrenkova K, Kaniakova M, and Horak M (2019). Lectins modulate the functional properties of GluN1/GluN3-containing NMDA receptors. Neuropharmacology 157, 107671. [PubMed: 31202607]
43. Crawley O, Conde-Dusman MJ, and Pérez-Otaño I (2021). GluN3A NMDA receptor subunits: more enigmatic than ever? J Physiol 600, 261–276. [PubMed: 33942912]
44. Das S, Sasaki YF, Rothe T, Premkumar LS, Takasu M, Crandall JE, Dikkes P, Conner DA, Rayudu PV, Cheung W, et al. (1998). Increased NMDA current and spine density in mice lacking the NMDA receptor subunit NR3A. Nature 393, 377–381. [PubMed: 9620802]
45. Pérez-Otaño I, Schulteis CT, Contractor A, Lipton SA, Trimmer JS, Sucher NJ, and Heinemann SF (2001). Assembly with the NR1 subunit is required for surface expression of NR3A-containing NMDA receptors. J. Neurosci 21, 1228–1237. [PubMed: 11160393]
46. Fiuza M, González-González I, and Pérez-Otaño I (2013). GluN3A expression restricts spine maturation via inhibition of GIT1/Rac1 signaling. Proc. Natl. Acad. Sci. USA 110, 20807–20812. [PubMed: 24297929]
47. Chamberlain SEL, González-González IM, Wilkinson KA, Konopacki FA, Kantamneni S, Henley JM, and Mellor JR (2012). SUMOylation and phosphorylation of GluK2 regulate kainate receptor trafficking and synaptic plasticity. Nat. Neurosci 15, 845–852. [PubMed: 22522402]
48. Chen BS, Gray JA, Sanz-Clemente A, Wei Z, Thomas EV, Nicoll RA, and Roche KW (2012). SAP102 mediates synaptic clearance of NMDA receptors. Cell Rep. 2, 1120–1128. [PubMed: 23103165]

49. Bellone C, and Nicoll RA (2007). Rapid bidirectional switching of synaptic NMDA receptors. Neuron 55, 779–785. [PubMed: 17785184]

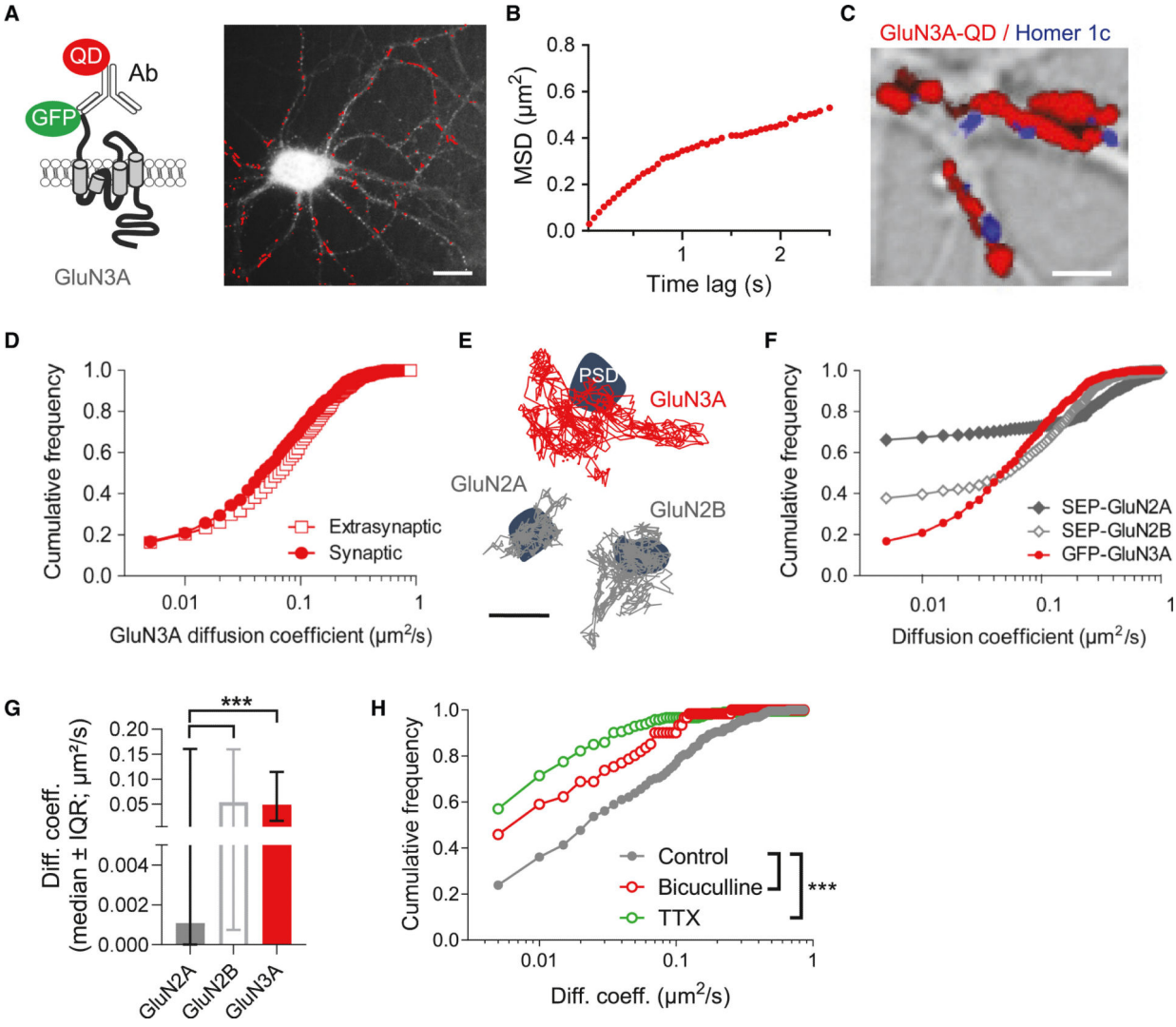

Figure 1. Surface diffusion of GluN3A-NMDARs in hippocampal neurons

(A) Surface GluN3A-NMDARs were detected using a quantum dot (QD)-antibody complex directed against the extracellular GFP tag, allowing high accuracy detection. Left: schematic showing single-particle tracking of surface GFP-GluN3A using QDs. Right: representative summed trajectories of GluN3A-QDs (red) acquired over a period of 30 s at a 20-Hz rate in a young (9 DIV) hippocampal neuron. Scale bar, 10 μm.

(B) Plot of the mean square displacement (MSD) vs. time for surface GluN3A-NMDARs (n = 143 trajectories, 44 fields from at least four different cultures) in young (7–9 DIV) neurons; dotted line is the behavior predicted for a freely diffusive receptor.

(C) Representative image of a dendritic field from a hippocampal neuron co-transfected with GFP-GluN3A and the postsynaptic marker Homer 1-DsRed (in blue). Summed QD trajectories for GluN3A-NMDARs are in red. Scale bar, 3 μm.

(D) Comparative cumulative distributions of the instantaneous diffusion coefficient of synaptic (n = 560) and extrasynaptic (n = 796, 47 fields from at least four different cultures) GFP-GluN3A receptors. Here and in subsequent figures, the first data point corresponds to the percentage of immobile receptors.

(E) Examples of reconstructed trajectories for transfected GFP-GluN3A, SEP-GluN2A, and SEP-GluN2B (SEP is a pH-sensitive variant of GFP). Scale bar, 1 μm.
(F) Cumulative distributions of the instantaneous diffusion coefficients of synaptic GFP-GluN3A (n = 560, 47 fields from at least four different cultures), SEPGluN2A (n = 1,009), and SEP-GluN2B (n = 1,531) in 7–9 DIV neurons ($p < 0.001$, Kruskal-Wallis followed by Dunn's post hoc test for all conditions).
(G) Comparison of the diffusion coefficients of synaptic GFP-GluN3A (n = 560 trajectories), SEP-GluN2A (n = 1,009 trajectories), and SEP-GluN2B (n = 1,531 trajectories). ***$p < 0.001$, Kruskal-Wallis followed by Dunn's post hoc test for all conditions.
(H) Cumulative distributions of the instantaneous diffusion coefficients of synaptic GFP-GluN3A in control (n = 285), TTX (n = 214), or bicuculline (n = 61) (***$p < 0.001$, Kruskal-Wallis followed by Dunn's post hoc test for all conditions).

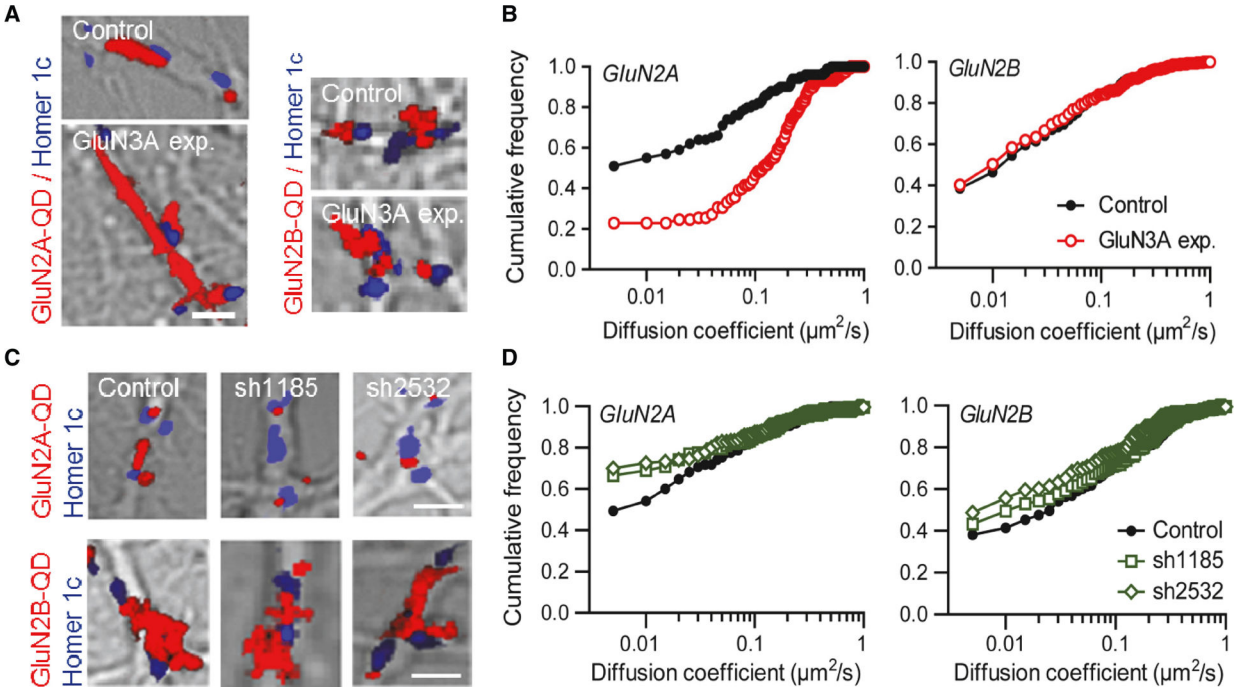

Figure 2. GluN3A subunit regulates the surface diffusion and synaptic retention of GluN2A-but not GluN2B-NMDARs

(A) Representative dendritic fields of 7–9 DIV hippocampal neurons transfected with Homer 1-DsRed (blue) and GFP-GluN3A, or control cells (expressing Homer 1 but not GFP-GluN3A), from the same preparation. Summed QD trajectories for native GluN2A-NMDARs and GluN2B-NMDARs are shown in red. Scale bar, 3 μm.

(B) Cumulative distribution of the instantaneous diffusion coefficients of synaptic GluN2A-QDs and GluN2B-QDs in control neurons (n = 89, 15 fields from at least three different cultures, and n = 306, nine fields, from at least three different cultures, respectively), and neurons expressing GFP-GluN3A (n = 119, 22 fields from at least three different cultures, and n = 277, 18 fields, from at least three different cultures) ($p < 0.0001$ for GluN2A, $p = 0.06$ for GluN2B; Mann-Whitney test).

(C) Representative dendritic fields of 7–9 DIV neurons transfected with Homer 1-DsRed (blue) and sh1185 or sh2532 as indicated. Summed QD trajectories for native GluN2A (top) and GluN2B (bottom) are shown in red. Scale bar, 3 μm.

(D) Cumulative distribution of the instantaneous diffusion coefficients of synaptic GluN2A-QDs and GluN2B at 7–9 DIV in control neurons (n = 85, 46 fields from at least six different cultures, and n = 181, 41 fields from at least six different cultures, respectively), and neurons transfected with sh1185 (n = 209, 38 fields from at least six different cultures, and n = 206, 38 fields from at least six different cultures) or sh2532 (n = 240, 37 fields from at least six different cultures, and n = 158, 33 fields from at least six different cultures) ($p < 0.006$ for GluN2A, $p = 0.08$ for GluN2B; Kruskal-Wallis followed by Dunn's multiple comparison test).

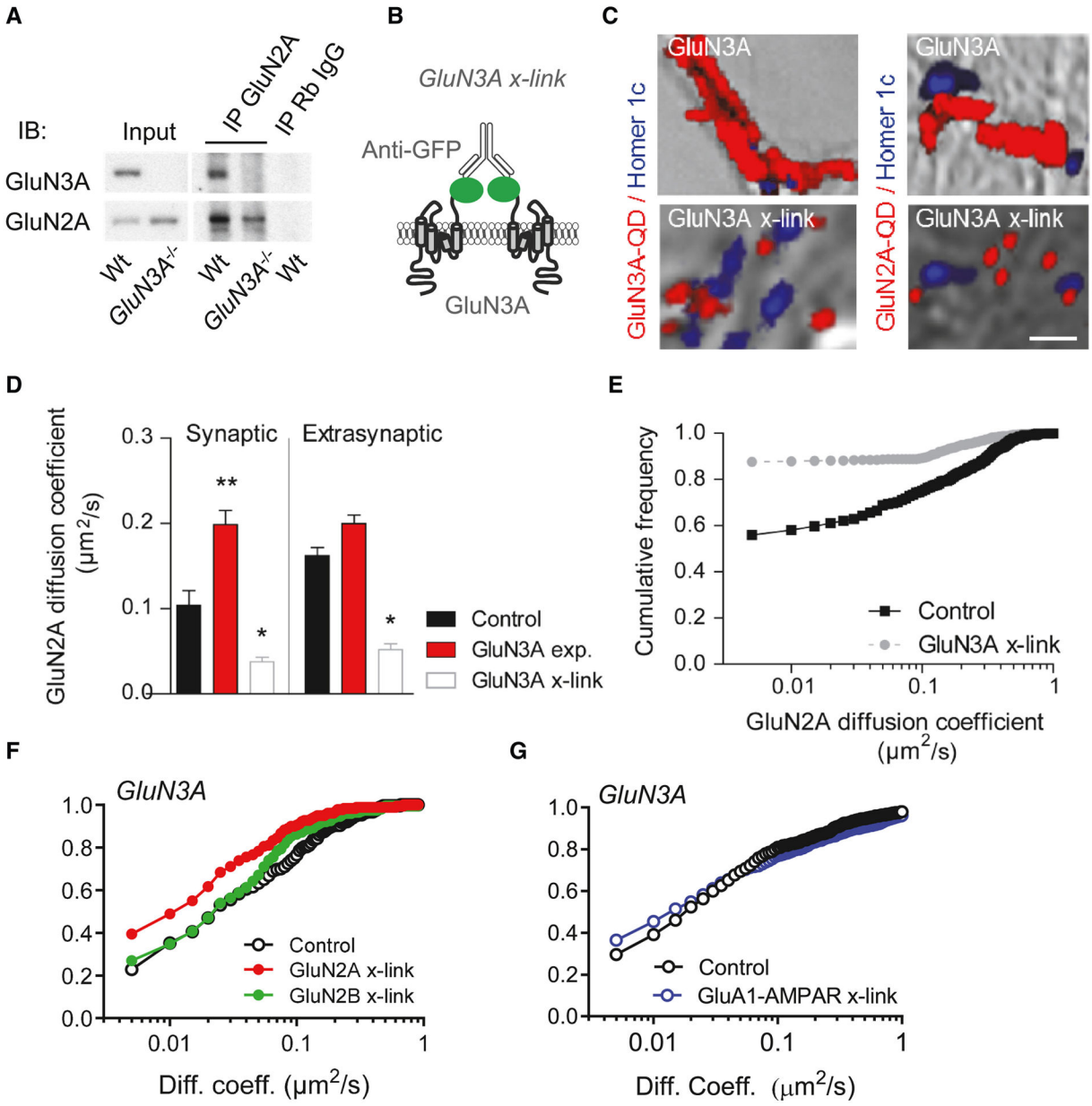

Figure 3. GluN3A subunit regulates synaptic GluN2A-NMDAR content

(A) Immunoprecipitation of GluN2A subunit from lysates of WT and *Grin3a*$^{-/-}$ cultured hippocampal neurons (9 DIV). Representative immunoblots (IBs) probed with the indicated antibodies are shown (n = 3 independent experiments).

(B) Schematic representation showing surface crosslinking (x-link) of GFP-GluN3A receptors with an antibody against the extracellular GFP tag, followed by a secondary antibody against immunoglobulin (Ig) G.

(C) Representative trajectories show reduced diffusion of QD-GluN3A-NMDARs after surface x-link relative to control in transfected 7–9 DIV hippocampal neurons. The surface immobilization of GFP-GluN3A also reduced GluN2A mobility. Scale bar, 2 μm.

(D) Average surface diffusion coefficients for synaptic (n = 52) and extrasynaptic (n = 292) GluN2A-NMDARs in control neurons (25 fields, at least three independent cultures) and in neurons overexpressing GFP-GluN3A with or without x-link (synaptic n = 359 and 94, extrasynaptic n = 432 and 320) (GFP-GluN3A, 47 fields from at least three independent cultures; GFP-GluN3A x-link, 34 fields from at least two independent cultures; ANOVA followed by Dunnett's multiple comparison test, *$p < 0.05$, **$p < 0.01$).
(E–G) Cumulative distributions of GluN2A-NMDAR (E) or GluN3A-NMDAR (F and G) instantaneous diffusion coefficients for synaptic trajectories in neurons transfected with GluN2 or GluN3A subunit and exposed to various x-link protocols (***$p < 0.001$ for GluN2A-NMDAR exposed to GluN3A x-link, Mann-Whitney test; $p > 0.05$ for all other conditions).

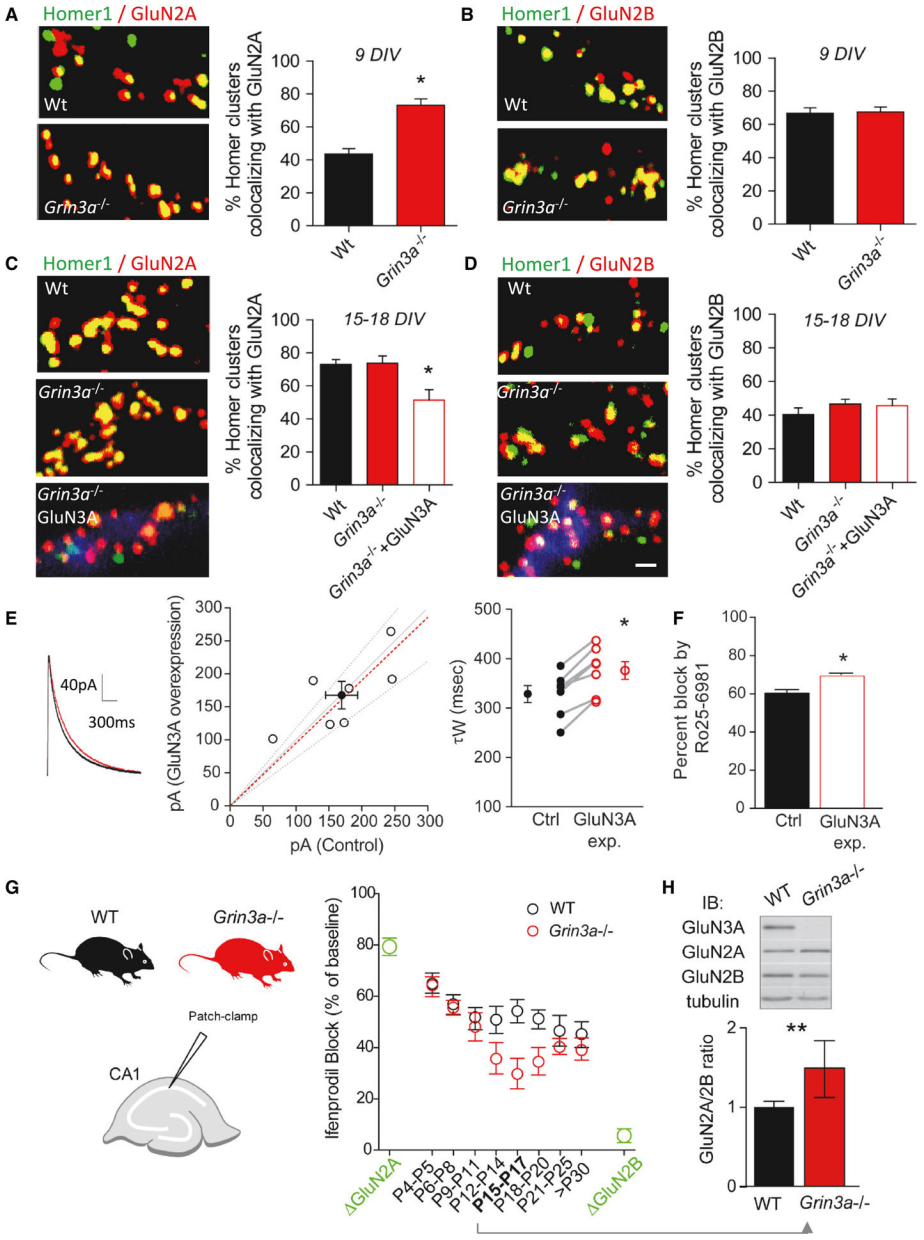

Figure 4. Developmental role of GluN3A subunit on the GluN2B-NMDAR relative abundance in synapse

(A–D) Co-localization analysis of surface GluN2A- or GluN2B-NMDARs (red) with Homer1 (green) in cultured hippocampal neurons from WT and *Grin3a*$^{-/-}$ mice at young (9 DIV) and more mature stages (15–18 DIV). Representative images and quantification (mean ± SEM) are shown (n = 3 independent experiments using different cultures, $p < 0.003$, Student's t test or ANOVA). Scale bar, 2 μm. In (C) and (D), *Grin3a*$^{-/-}$ neurons were transfected with GFP-GluN3A (blue) when indicated.

(E) Organotypic hippocampal slice cultures from P7 rats were biolistically transfected with GFP-GluN3A subunit on DIV 3–4, and simultaneous whole-cell recordings obtained from transfected and neighboring CA1 pyramidal neurons on DIV 7. Left, sample traces of NMDAR-EPSCs from a control (black) and a GFP-GluN3A transfected cell (red). Middle,

scatterplots of peak amplitudes of NMDAR-EPSCs from single pairs (open circles) and mean ± SEM (filled circle) from transfected and control cells (mean amplitude [pA]: control 169.5 ± 24.3, transfected 168.0 ± 21.0, n = 7). Dashed lines represent linear regression and 95% confidence interval. Right, NMDAR-EPSC decay times from cell pairs expressed in milliseconds as a weighted tau (τ_w) from paired transfected and control cells (mean decay: control 328.7 ± 17.1 ms, transfected 376.3 ± 18.0 ms, n = 7, p = 0.0002 by paired Student's t test).

(F) Percentage of block of NMDAR-EPSCs by the GluN2B selective antagonist Ro25–6981 (n = 5, p = 0.027, paired Student's t test).

(G) Schematic representation of the experimental design (left panel). Developmental time course of ifenprodil sensitivity of NMDAR-EPSCs from CA1 pyramidal neurons from WT (black circles) or *Grin3a*$^{-/-}$ mice (red circles), represented as the percentage decrease in peak current after ifenprodil. For comparison, data from Gray et al.[35] of the ifenprodil sensitivity data of "pure" synaptic populations of GluN2A and GluN2B are included (green circles).

(H) Western blot measurement at P15–17 of GluN2A and GluN2B subunit content in WT and *Grin3a*$^{-/-}$ mice.

KEY RESOURCES TABLE

REAGENT or RESOURCE	SOURCE	IDENTIFIER
Antibodies		
Mouse monoclonal anti-GFP (3E6)	Thermo Scientific	Cat# A-11120
Rabbit anti-GluN2A (extracelular)	Alomone Labs	Cat# AGC-002
Rabbit anti-GluN2B (extracelular)	Alomone Labs	Cat# AGC-003
Goat polyclonal anti-GFP	Abcam	Cat# ab5450
Goat anti-Homer1 b/c	Santa Cruz Biotechnology	Cat# sc-8923
Mouse anti-PSD95	Merck Millipore	Cat# CP35
Rabbit anti-GluN2A	Merck Millipore	Cat# M264
Goat anti-EphB2R	R&D	Cat# AF467
Rabbit anti-GluN3A	Merck Millipore	Cat# 07-356
Rabbit anti-GluN2B	Merck Millipore	Cat# AB1557
Biological samples		
Hippocampal cultured neurons	This paper	N/A
Chemicals, peptides, and recombinant proteins		
Tetrodotoxin (TTX) citrate	Bio-Techne	Cat #1069/1
(−)-Bicuculline methiodide	AbCam	Cat# Ab120108
Protein A/G agarose beads	Pierce	Cat# 10540424
F (ab')2-Goat anti-Rabbit Qdot655	ThermoFisher Sc.	Cat# Q11422MP
Ro 25-6981	Merck Millipore	Cat# R7150
Ifenprodil	Tocris	Cat# 0545
Experimental models: Organisms/strains		
Sprague-Dawley rats	Janvier labs	N/A
Mouse: B6;129 3 1-Grin3atm1Nnk/J, crossed for 12 generations into a C57Bl6J background	Provided by Nakanishi and Lipton[44]	N/A
Recombinant DNA		
pCIneo-GFPGluN3A	Perez-Otano et al.[45]	N/A
sh3A2532 in pSuper-GFP	Kehoe et al.[17]	N/A
sh3A1185 in pSuper-GFP	Kehoe et al.[17]	N/A
Software and algorithms		
SigmaStat software	Addlink	https://www.addlink.es/productos/sigmastat
MetaMorph software (7.8.9.0)	Molecular Devices	https://www.moleculardevices.com/systems/metamorph-research-imaging/metamorphmicroscopy-automation-and-image-analysis-software